

Surface-Functionalized Cellulose Nanocrystals as Nanofillers for Crosslinking Processes: Implications for Thermosetting Resins

R. Haney, L. Wiegart

To be published in "ACS APPLIED NANO MATERIALS"

February 2022

Photon Sciences

Brookhaven National Laboratory

U.S. Department of Energy

USDOE Office of Science (SC), Basic Energy Sciences (BES) (SC-22)

Notice: This manuscript has been authored by employees of Brookhaven Science Associates, LLC under Contract No. DE-SC0012704 with the U.S. Department of Energy. The publisher by accepting the manuscript for publication acknowledges that the United States Government retains a non-exclusive, paid-up, irrevocable, world-wide license to publish or reproduce the published form of this manuscript, or allow others to do so, for United States Government purposes.

DISCLAIMER

This report was prepared as an account of work sponsored by an agency of the United States Government. Neither the United States Government nor any agency thereof, nor any of their employees, nor any of their contractors, subcontractors, or their employees, makes any warranty, express or implied, or assumes any legal liability or responsibility for the accuracy, completeness, or any third party's use or the results of such use of any information, apparatus, product, or process disclosed, or represents that its use would not infringe privately owned rights. Reference herein to any specific commercial product, process, or service by trade name, trademark, manufacturer, or otherwise, does not necessarily constitute or imply its endorsement, recommendation, or favoring by the United States Government or any agency thereof or its contractors or subcontractors. The views and opinions of authors expressed herein do not necessarily state or reflect those of the United States Government or any agency thereof.

Surface-Functionalized Cellulose Nanocrystals as Nanofillers for Crosslinking Processes: Implications for Thermosetting Resins

Roneisha Haney¹, Ravichandran H. Kollarigowda¹, Lutz Wiegart², and Subramanian Ramakrishnan^{1}*

¹Department of Chemical and Biomedical Engineering, FAMU-FSU Engineering, Tallahassee, Florida 32310, USA.

²National Synchrotron Light Source II, Brookhaven National Laboratory, Upton, New York 11973, USA

*Subramanian Ramakrishnan (srama@eng.famu.fsu.edu)

KEYWORDS cellulose nanocrystals, x-ray photon correlation spectroscopy, epoxy composite, thermosetting resins, filler dynamics, curing kinetics

ABSTRACT

Understanding the response of fillers in the epoxy resin crosslinking process and characterizing polymer-filler dynamics are key features that guide the engineering of new thermosetting resin composites. In this work, X-ray photon correlation spectroscopy (XPCS) is used as a thermal analysis tool to track the microscopic changes occurring during the cure of a functionalized cellulose nanocrystal (mCNC)-epoxy composite. In contrast, traditional methods such as differential scanning calorimetry (DSC) and curing rheology are used to understand the kinetics and properties on macroscopic length scales. Of interest is the influence of the mCNC on the curing

kinetics and properties of the thermosetting resin. Two levels of modification (increasing hydrophobicity) were chosen to observe the effect of functionalization. Before cure, the highly functionalized CNC (mCNC3) shows a 44% increase in complex viscosity (η^*), while the less functionalized CNC (mCNC2) shows a similar η^* value to the neat resin. As the cure cycle progresses, results from DSC, rheology, and XPCS further show the enhancement in dispersion for mCNC3. The results show a clear difference in the maximum drift velocity, maximum heat flow, and complex viscosity during the ramp to the isothermal cure temperature (T_{cure}). Such results suggest that mCNC3 contains a well-dispersed network of particles due to the higher level of functionalization. During T_{cure} , a transition in elastic modulus (G') occurs only for the highly functionalized CNC particle system. We believe that heat-induced aggregation occurs, and the crosslinked resin ultimately dominates the macroscopic properties of the final cured system for all samples. The results from the three techniques are in good agreement and showcase XPCS as a beneficial experimental tool for characterizing the microscopic dynamics of particulate-filled thermosetting resins. Hence, we envision this to be a fundamental curing study for the design of thermosetting resin composites.

INTRODUCTION

Epoxy resins show several advantages compared to other polymers, including high mechanical strength, corrosion resistance, and ease of processability.¹ The high-performance properties and versatility of epoxy resins allow the material to be used for structural applications, adhesives, corrosion-resistant coatings, and more.² To expand epoxy resins applications further, nano- and micro-sized fillers are often incorporated into the epoxy resin. Fillers such as carbon fiber, glass fibers, and carbon nanotubes have been widely used to increase epoxy resins' toughness, conductivity, strength, and other performance properties.^{3,4} In addition to the fillers mentioned,

cellulose nanocrystals (CNCs) have recently been explored as potential filler materials in polymeric nanocomposites.^{5,6} The anisotropic, rod-like crystalline materials are biodegradable, renewable in nature, lightweight, and are quickly processed. CNCs have comparable performance properties to the more commonly used fillers but have a significantly lower cost.⁷ The lower manufacturing and processing costs of CNCs make them an ideal low-cost, high-performance filler material to be used to produce functional, lightweight, advanced composites^{8,9}.

Furthermore, CNCs have an abundance of -OH groups on the nanoparticle's surface that allow for a wide range of functionalization.¹⁰ Several groups have used different functionalization techniques to adjust and alter the level of hydrophilicity of CNCs, thus allowing them to be dispersed into a broader range of solvents and polymer matrices.¹¹⁻¹⁴ One common technique used to increase the hydrophobic nature of CNCs is surface esterification^{15,16}.

Esterification is a chemical reaction in which two reactants (typically an alcohol and an acid) form an ester as the reaction product.¹⁷ Regarding CNCs, the -OH groups serve as the alcohol, and an acid, such as acyl chloride, stearoyl chloride, or lauroyl chloride, serves as the second reactant.¹⁸ At the end of the reaction, the hydroxyl groups are converted to esters, resulting in a CNC with less hydrophilic properties.¹⁶ The level of hydrophobicity depends directly on the amount of acid present during the reaction. Tailoring of the surface chemistry of CNCs allows for dispersion into non-polar, hydrophobic mediums, such as epoxy resins.^{16,19} After the CNC has been modified and dispersed into the desired matrix, it is necessary to understand how the two interact. Several works have been dedicated to understanding filler-matrix interactions and how they translate to changes in the overall macroscopic properties.¹⁹⁻²³

During the cure of the epoxy resin, a network is built due to the formation of crosslinks. These crosslinks directly contribute to the final macroscopic properties.²⁴ The crosslinks are formed in

two different steps. First, epoxy groups react with the amine-hydrogen, resulting in the formation of a hydroxyl group. In the second step, the linking of chains occurs due to the amine-hydrogen groups' presence at the end of the molecular chains.²⁵ This process continues until amine-hydrogen groups are no longer available. Incorporating CNCs into this two-part thermosetting resin is of interest to enhance the neat system's macroscopic properties. However, the presence of the CNCs during the crosslinking reaction will influence and affect the rate at which the crosslinked epoxy network is formed.

Different experimental techniques can be used to investigate the curing kinetics and thermal transitions that occur during the crosslinking of composites based on thermosetting resins. Differential scanning calorimetry (DSC) and rheology are two standard methods used to explore and track macroscopic changes during the formation of the crosslinked network within epoxy resins.²⁶⁻³¹ However, few works have been dedicated to understanding the effect of fillers on creating this crosslinked network. Furthermore, the reactions during the thermal cure of epoxy resins are complex due to the several reactive processes co-occurring.³²

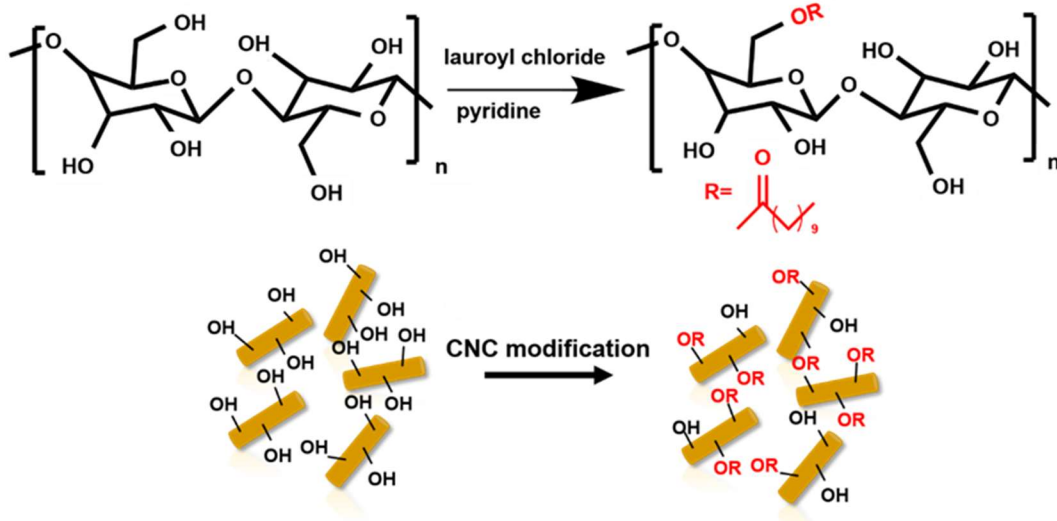
Incorporating a filler amid this reaction can complicate the analysis and interpretation of the results. Therefore, other experimental techniques must be explored to understand the effect fillers have on the thermal transitions within the composite. In a recent study, X-ray photon correlation spectroscopy (XPCS) is used to track the curing reaction of LOCTITE 3536 CSP, an industrial epoxy adhesive³³. The formulation contained 25 wt% alumina fillers (polydisperse with a mean diameter $\sim 2 \mu\text{m}$) as a marker to resolve the dynamics of the epoxy during the curing process. The results showed a correlation between the exothermic heat released during DSC measurements and the nanoscale changes in dynamics during the isothermal cure. As the reaction proceeds (as measured with DSC), the dynamics rapidly slows down.

Nevertheless, a complete elucidation of the dynamics of mCNC type of fillers in thermosetting resins that considers all the problematic aspects is still lacking. With XPCS, the thermoset composite's dynamical properties can be studied through the motion of the nanoparticles within the resin.³⁴⁻³⁶ During XPCS measurements, electron density gradients cause X-rays to scatter within the functionalized CNC-epoxy system.³⁷ This scattered X-ray gives rise to a scattering image or speckle pattern. It is expected that the arrangement of the CNCs will change with time, and this dynamic behavior results in a change in the speckle pattern over time.

In thermosetting resins, filler dynamics or aggregation processes occur at the macromolecular level and still need to be better understood. This work investigates surface-functionalized cellulose nanocrystals' (mCNC) influence on a commonly used epoxy resin's curing kinetics and macroscopic properties (EPON 828). A particular interest lies in a possible change in the structure and arrangement of the highly loaded cellulose nanocrystals during post-processing. To understand and track the changes that occur during the formation of the three-dimensional network in the presence of the mCNCs, XPCS will be employed to study the dynamical properties of the three-component (mCNC, resin, crosslinking agent) system. The results from the XPCS will provide qualitative and quantitative information regarding the cure behavior of the CNC-epoxy composite and are used to corroborate information obtained from traditional thermal analysis techniques such as DSC and curing rheology. While DSC and rheology are reliable tools for understanding macroscopic properties such as degree of cure, gel point, and elastic modulus. XPCS can provide additional information to better understand the composite's properties at the nanoscale. Several studies showcase enhanced dispersion of CNCs after modification^{12,13,16,19}. However, there are no reported studies on how this dispersion changes during post-processing.

RESULTS AND DISCUSSION

a)



b)

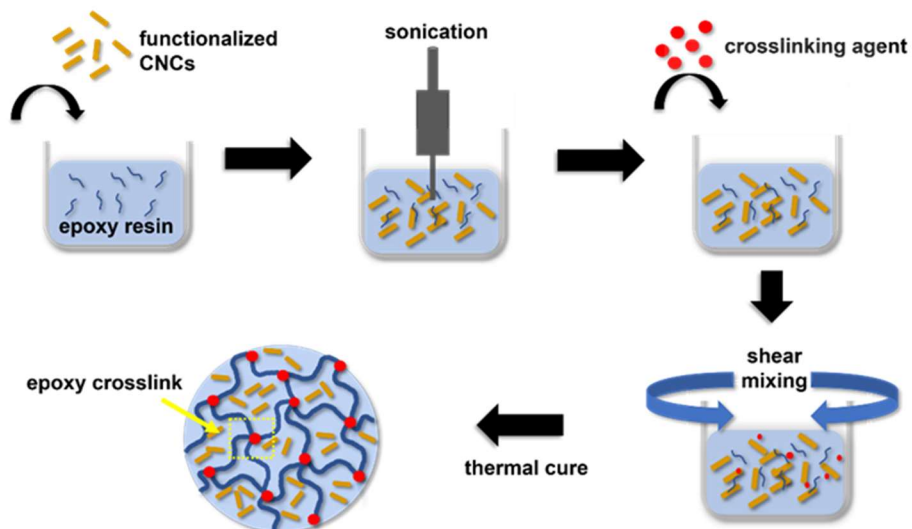


Figure 1. Schematic illustration of (a) chemical structures of CNC surface modification. (b) mCNC dispersion and formulation method and final crosslinked state of the composite after thermal cure. In the schematic representation of the modified CNC in epoxy resin composite, gold represents the CNC particles, blue represents the epoxy resin, and the red segments correspond to the crosslinking agent.

CNC surface modification

To study the effect of the CNC's hydrophobic surface, two different degrees of substitution have been obtained upon modification shown in Figure 1a. Transmission electron microscopy is used to confirm the rod-like shape of the CNCs, while Fourier transform infrared spectroscopy (FTIR)

and x-ray diffraction (XRD) confirmed the differences in the levels of surface modification. In addition, dispersibility tests show changes in the compatibility of the mCNCs in various solvents, and small-angle x-ray scattering (SAXS) measurements provided insight into the overall structure of the mCNCs once dispersed in the epoxy resin.

The TEM image of the unmodified CNCs is shown in Figure S1, where the average length and width are 126 ± 41 and 13 ± 3.8 nm, with an average aspect ratio of ~ 10 . The mCNCs functionalization with lauroyl chloride was qualitatively confirmed using FTIR and XRD. Figure S3 shows the XRD pattern and the FTIR spectra of the neat and modified CNC powders. The FTIR spectra show a broad peak from $3600\text{--}3200\text{ cm}^{-1}$ due to the CNC's surface's hydroxyl groups.^{10,16} This peak is evident for all samples, which shows that even at the highest level of the modification (10%), -OH groups are still present. However, the most notable change was the appearance of the peak at 1743 cm^{-1} , corresponding to the carbonyl C=O stretching from the CNC grafted lauroyl chloride.¹⁶ The XRD pattern for the neat CNC shows the expected characteristic diffraction peaks at 2θ values (and their corresponding plane) of 14.9° (100), 16.5° ($101\bar{1}$), 22.7° (002), and 34.5° (004).^{10,38-41} The observed peaks correspond to the typical reflection planes of the CNC. After modification, a new peak appears around 20° . This peak is most evident for the mCNC2 (7%) and mCNC3 (10%) modification and corresponds to the fatty acid chain grafted on the CNC's surface^{16,42}. Furthermore, the intensity of the peaks from the diffraction pattern can be used to calculate the crystallinity index (CI) of the neat and modified CNCs (Table S1). After modification, the minimal change in CI suggests that the crystalline particle maintained its original structure despite removing -OH groups during the esterification reaction.^{16,43}

CNCs dispersion in solvents and epoxy resin

After modifying the CNCs, the dried CNCs (unmodified and modified) were dispersed into various solvents with varying polarities (water, ethanol, DMSO, acetone, toluene, and cyclohexane). The

images are shown in Figure S4. The naturally hydrophilic CNC is readily dispersed in water (Figure S4a). The hydrophilicity of CNC is owed to the abundance of hydroxyl groups on the surface. In the remaining solvents, the unmodified, naturally hydrophilic CNC either forms a cloudy mixture, or complete sedimentation occurs (see Figure S3b-f). The CNC modification involved an esterification reaction, resulting in grafting of a hydrophobic fatty acid, lauroyl chloride. The highly modified CNC (mCNC3) formed homogeneously dispersed suspensions in toluene and cyclohexane (see Figure S3e-f), showcasing a CNC particle with hydrophobic properties.

Following confirmation of the surface modification, the mCNCs were then dispersed into the mostly non-polar epoxy resin, and the structure of the two modified systems (mCNC2, mCNC3) were assessed using SAXS, which is performed simultaneously during XPCS measurements. During the measurement, electron density gradients cause x-rays to scatter within the disordered CNC-epoxy system, giving rise to a diffraction image (speckle pattern).⁴⁴ The changes in intensity as a function of q provide a direct assessment of the nanostructure of the CNCs. The two-dimensional SAXS images (Figure S5) showed isotropic, circular patterns; therefore, results were azimuthally averaged to obtain intensity, I , versus wavevector, q , plots. The I vs. q plots for mCNC2 and mCNC3 at 25°C are shown in Figure 2. The modeling and interpretation of the I vs. q data can be challenging due to the high level of polydispersity, the anisotropic rod-shaped CNC particle, and the high loading of the CNCs.^{35,45-47} However, extraction of the power-law exponent, where $I(q) \propto q^{-p}$ can provide key information about the CNC's general nature and overall cluster size. As shown in Figure 2, mCNC2 and mCNC3 have different p values of 3.39 and 2.47 at low q values ($q < 0.0015 \text{ \AA}^{-1}$). This trend is consistent throughout the cure, as shown in Figure S6. The p -value associated with mCNC2 is directly correlated to the presence of larger aggregates. It is

expected that mCNC2 would have larger clusters due to the increased attractive forces amongst the CNC particles and the lack of compatibility in the mostly non-polar resin. An increase in the p-value is often observed when larger clusters are formed and coupled with the essential "loss" of the primary particle.⁴⁸ This specific arrangement should be avoided for systems that desire gelation, as this arrangement can prevent percolation and the formation of a structured network.^{48,49}

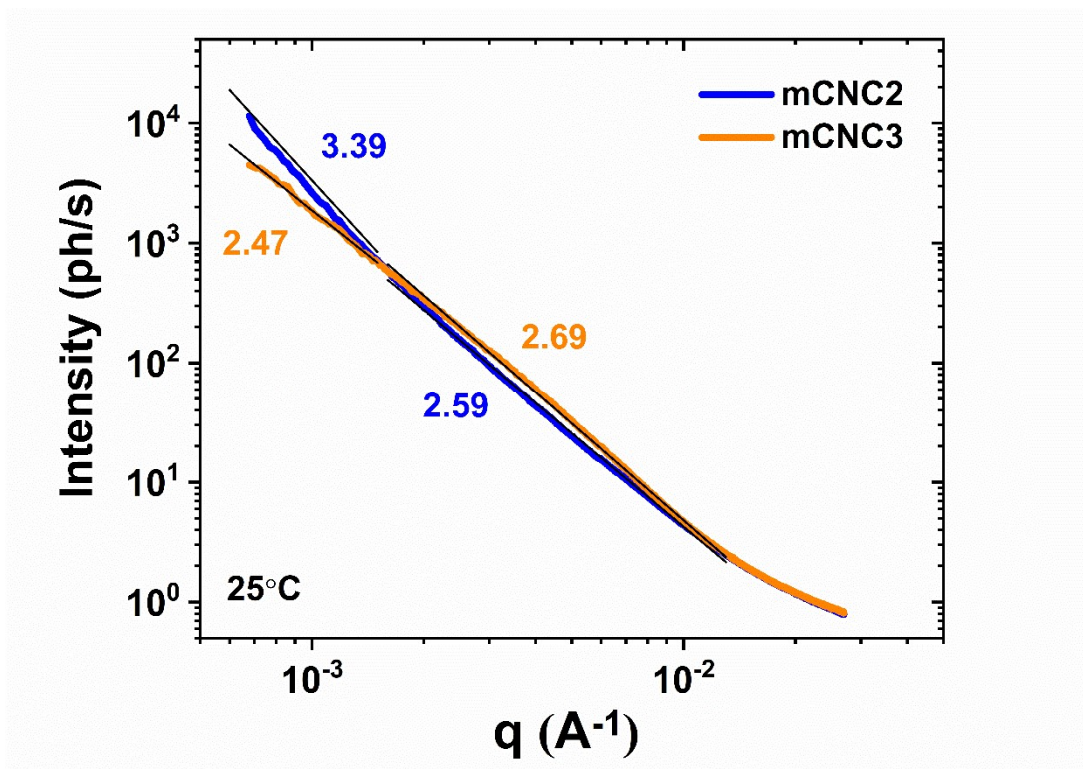


Figure 2. Small-angle x-ray scattering measurements and power-law fits of mCNC samples. The intensity (I) vs. q plots for mCNC2 and mCNC3 are shown at the beginning of cure (25°C) with the corresponding power-law fits (p) where $I(q) \propto q^{-p}$.

At $q > 0.0015 \text{ \AA}^{-1}$, the mCNC2 and mCNC3 curves overlap. The curves overlap shows that the most prominent differences in structure are on larger length scales ($q < 0.0015 \text{ \AA}^{-1}$), and the clusters formed within mCNC2 and mCNC3 are composed of similar intermediate structures. Additionally, the variations in the power-law dependence as a function of q indicate a system of CNCs comprised of varying microscopic structures.⁵ The results from the SAXS measurements confirm the changes

in structure (mCNC2 vs. mCNC3) and indicate the presence of larger aggregates in the sample containing the less modified CNC.

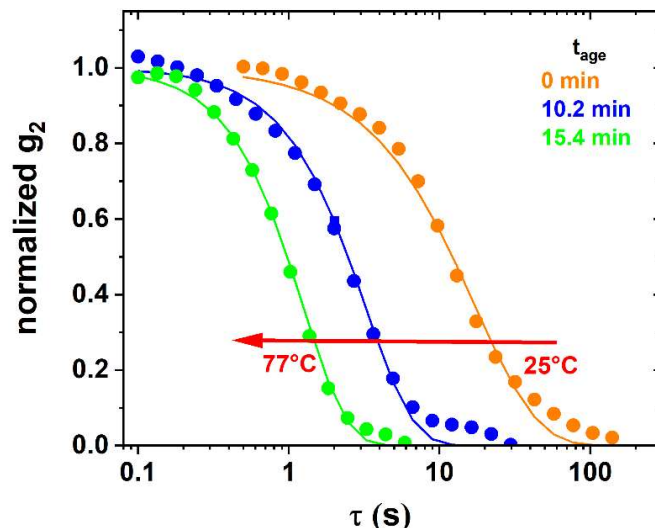
Dynamics of CNCs during thermal cure

XPCS was used in this study to reveal the effect of surface-modified CNCs on the nanoscale properties of EPON 828 during crosslinking and, thus, to showcase the use of XPCS as a valuable technique for understanding the thermal curing of polymeric nanocomposites. During XPCS measurements, the nanoscale motion of the rod-like mCNC is measured. We believe that this motion can be directly related to the evolution of the epoxy-amine network surrounding the mCNCs.³⁴ We measure dynamical properties during the composites' thermal cure to understand thermally induced transitions in the mCNC2 and mCNC3 samples.

At $t_{\text{age}}=0$ min, the temperature ramp ($5^{\circ}\text{C}/\text{min}$) to 90°C starts from room temperature ($\sim 25^{\circ}\text{C}$). After 13 min, the sample reaches 90°C , and the isothermal cure starts. In Figure 3 (a-b), the one-time correlation functions according to Equation (2) are shown throughout the cure cycle of mCNC2. The correlation functions shown in Figure 3 were obtained for $q=0.0061 \text{ \AA}^{-1}$, corresponding to a length scale of about 100nm. The evolution of g_2 is distinct during the temperature ramp from 25 - 90°C and during the isothermal cure at 90°C . During the ramp, the dynamics speed up until the sample reaches 90°C . This is shown through a shift in the g_2 curves to the left. After the temperature reaches 90°C , the g_2 curves shift to the right, and the value of τ_0 starts increasing with time. While the τ_0 values obtained by fitting the correlation functions with Equation (2) represent the dynamics of the mCNC, it also serves as an indirect measurement of

the epoxy crosslink formations. Consequently, as the epoxy crosslinks form, the movement of the mCNC is restricted, resulting in slower dynamics.

a)



b)

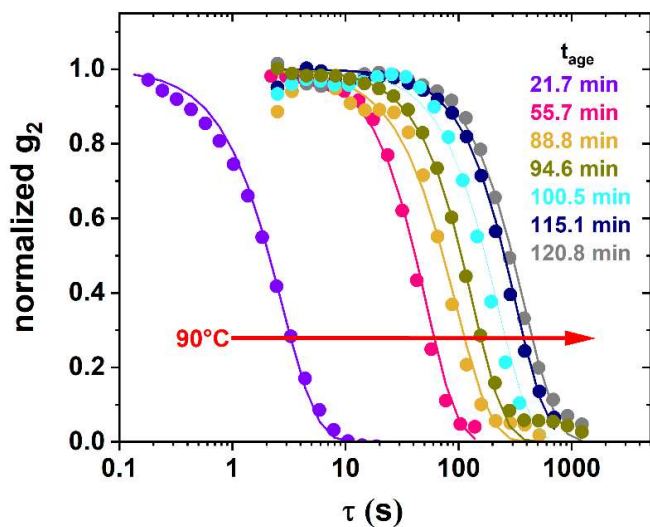


Figure 3. XPCS one-time autocorrelation function g_2 during the isothermal cure for the mCNC2 sample from (a) 25-77°C and (b) throughout the isothermal cure at 90°C.

mCNC2 and mCNC3 display different τ_0 values at 25°C, where mCNC2 exhibits faster dynamics ($\tau_0=29.5$ s) than mCNC3 ($\tau_0=77.6$ s). At room temperature, there is no significant influence of viscous forces from the polymer or the formation of crosslinks, which means that the differences in the dynamics are purely due to the network of dispersed CNCs. At $t_{\text{age}}=15.4$ minutes, the sample reaches a temperature of 77°C. During the ramp, τ_0 decreases for both mCNC2 ($\tau_0=2.27$ s) and mCNC3 ($\tau_0=12.41$ s) at $q=0.0061$ Å⁻¹. This decrease in τ_0 attributes to an increase in the thermal motion of the epoxy resin. The higher τ_0 value displayed in mCNC3 (compared to mCNC2) showcases the competition between the polymer's viscous forces and the elastic properties of the CNC network. The polymer's thermal motion is less evident in mCNC3, where the CNCs are better dispersed. In contrast, mCNC2 yields a significantly faster τ_0 due to a more aggregated network of CNCs, resulting in more dominant viscous forces from the epoxy resin.

While the discussion above regarding τ_0 is specific to a particular q value, it is also imperative to assess the change in dynamics as a function of the wave vector, q . The q -dependent dynamics give insight into whether the motion is diffusive or ballistic.^{37,50} As shown in Figure S7, we find the q -dependence of τ_0 to be linear throughout the entire cure, where $\tau_0=v_d^{-1}q^{-1}$. v_d , also known as drift velocity, describes the ballistic motion of the mCNCs.³³ This linear dependence on q , as opposed to the power-law dependence seen in diffusive systems, is typical for systems with highly interacting colloids.⁵¹ By tracking the drift velocity of the system during the cure, the nanoscale dynamics are revealed.

Figure 4 shows the evolution of v_d for mCNC2 and mCNC3. At $t_{\text{age}}=0$, there is an order of magnitude difference of the v_d values shown in mCNC2 (2.3 nm/s) and mCNC3 (0.13 nm/s). The higher v_d value associated with mCNC3 suggests the dynamics are faster than those of mCNC2. The slower dynamics observed in mCNC3 are due to an organized and well-spanned network of

CNCs. We attribute this enhancement in dispersion to the higher level of modification imparted on the CNC's surface. During the temperature ramp to 90°C, v_d quickly increases for both mCNC2 and mCNC3. The faster dynamics are also shown through the changes in τ_0 discussed earlier. For the mCNC3 sample, where the CNC network is most prevalent and well dispersed, the maximum drift velocity is slightly lower than that of the mCNC2.

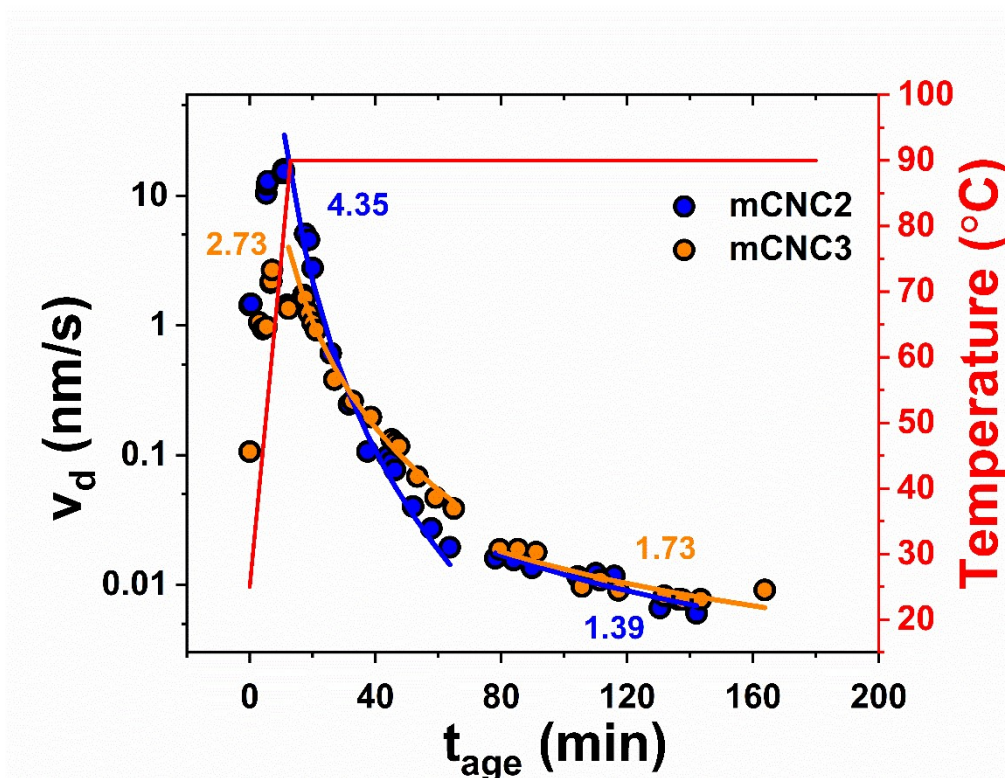


Figure 4. XPCS dynamics measurements during the thermal cure of the mCNC samples. Local velocity ($\tau_0=v_d^{-1} q$) is measured for mCNC2 and mCNC3, and the corresponding time-dependent power-law fits are shown, where $v_d \propto t_{age}^{-n}$.

Once we reach the isothermal cure temperature $T=90^\circ\text{C}$ ($t_{age}>13$ min), a power-law fit is used to quantitatively compare the changes, where $v_d \propto t_{age}^{-n}$. In the t_{age} region 13 to 73 min, there is a clear difference in the power-law exponent for mCNC2 ($n=4.35$) compared to mCNC3 ($n=2.73$). The faster decrease of v_d for mCNC2 compared to mCNC3 is a direct consequence of the underlying

microstructure. The more dispersed state of the CNCs in mCNC3 prevents the formation of crosslinks, thus slowing the reaction rate and a more gradual reduction in v_d . As expected, the aggregated and larger structures present in mCNC2 allow the more rapid crosslinking of the resin (cellulose is not in the way of the resin as in mCNC3), resulting in a more rapid decrease in v_d . Finally, at $t_{age}=135$ min, both modified systems' drift velocity plateau reaches the exact value of 6.4×10^{-3} nm/s. The identical final v_d values imply that the modified system's final nanoscale properties are the same despite the difference in dynamics before and during the cure cycle.

In addition to τ_0 , we can also gain insight into the nature of the dynamic processes by extracting the stretching exponent, γ , of the exponential decay function (see Equation 2). $\gamma > 1$ for a compressed exponential function, $\gamma < 1$ for a stretched exponential function, and $\gamma = 1$ for a simple exponential function.³⁷ In this study, $\gamma > 1$ throughout the entire cure cycle (Figure S8). Thus, the sample's relaxation is faster than exponential. The ballistic motion combined with the compressed shape of g_2 is commonly observed in colloidal gels, emulsions, concentrated samples, and suspensions.⁵²⁻⁵⁸ This integrated feature is often attributed to elastic strain within systems due to heterogeneous internal stresses.^{56,59,60} The quantitative and qualitative results from the one-time and two-time autocorrelation functions provide additional insight into the nanoscale motion changes that occur in the CNC-epoxy composite during thermal cure. Additionally, results from the SAXS measurements confirm the nanoscale changes. The faster τ_0 and v_d values in mCNC2 are due to the formation of isolated clusters of CNCs (compared to mCNC3) and a more significant impact during cure from the viscous epoxy resin.

DSC Thermal Analysis

While XPCS provides information about changes during curing on the nanoscale, DSC is a traditional thermal analysis tool used to understand macroscopic changes of thermosetting

resins.^{27,61} DSC provides information regarding the thermal transition points within the cure cycle. In a study done by Yavitt et al., researchers correlate the heat generated during post-processing of a thermally cured epoxy resin and directly related to the changes in drift velocity obtained from XPCS studies. This study explores this theory further with functionalized particles, where mCNC2 and mCNC3 are isothermally cured at 90°C for 120 minutes. During this study, the heat flow was measured over time. The results are shown in Figure 5 and display the effect of surface modification (mCNC2 vs. mCNC3) on thermal properties. There is a decrease in the maximum heat flow when the surface modification is increased. The heat flow or reaction rate is the highest at the beginning of the isothermal cure when the sample reaches 90°C. A maximum heat flow is observed when the unreacted material concentration is highest.⁶² mCNC2 and mCNC3 each contain a CNC loading of 15.5vol%. However, mCNC3 shows a lower maximum heat flow due to the network of CNCs throughout the matrix.

Additionally, the inset figure (Figure 5) highlights the differences in the initial decay of the heat flow. The power-law fit displays a faster decay of heat flow for mCNC2 (4.00) as compared to mCNC3 (2.59). The differences in the decay of heat flow can be correlated to the variations in structure between the two modified systems. In mCNC2, where the system is comprised of aggregated CNCs, heat can readily flow throughout the system. This increases exothermic heat, allowing for the reaction to proceed more rapidly. For mCNC3, where the particles are better dispersed, the heat flow throughout the epoxy matrix is slower due to the presence of the CNCs,

resulting in a 'delay' of crosslinking and a slower decay of heat flow. As the crosslinking process proceeds and all the epoxy crosslinks are formed, the heat flow decreases and plateaus to zero.

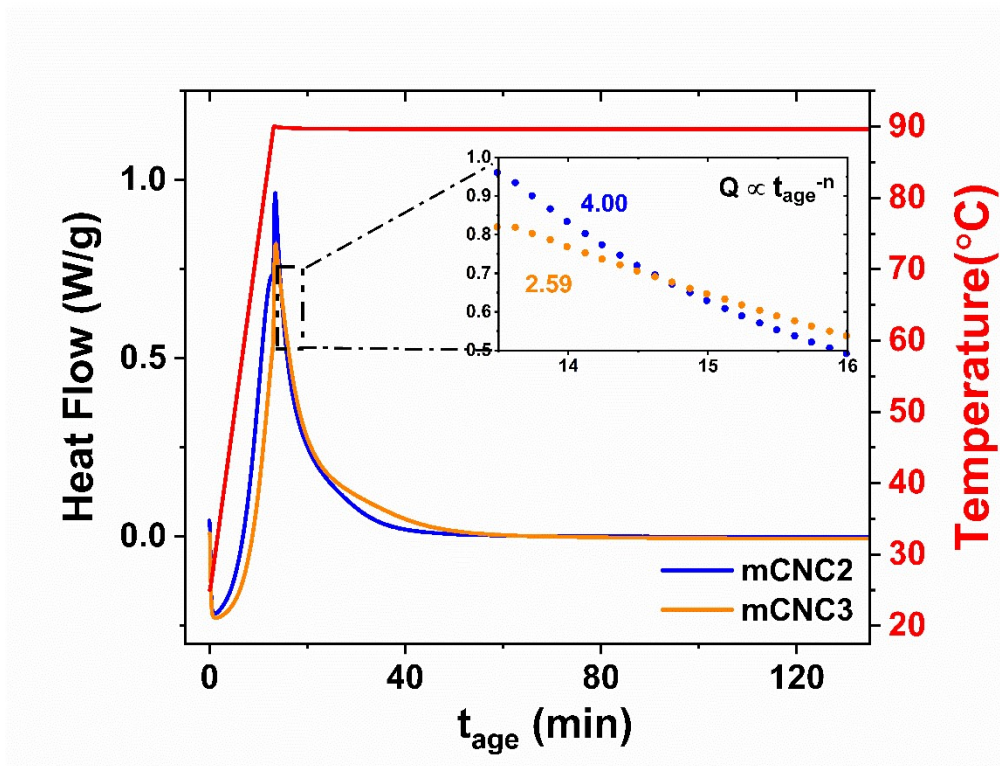


Figure 5. Isothermal DSC thermograms of the mCNC samples heated at 5°C/min and held at 90°C for 120 minutes. The embedded plot (top right) shows a power-law fit ($Q \propto t_{\text{age}}^{-n}$) expressing the differences in the initial decay of the heat flow at the start of the isothermal cure.

Curing Rheology

In addition to DSC, curing rheology is often used to understand the formation of the crosslinked network within epoxy resins.⁶³ The construction of the three-dimensional network can be tracked by observing the viscoelastic behavior over time.⁶⁴ The measurement of complex viscosity (η^*), modulus (storage- G' and loss- G''), and gel time (t_{gel}) were employed to trace any changes in structure that occur during thermal crosslinking. In the rheology experiments, at $t_{\text{age}}=0$ min (as in

XPCS and DSC), the temperature ramp is started at 25°C to heat to 90°C (5°C /min). At a t_{age} of 13 min, a temperature of 90°C is reached.

In Figure S10, the evolution of the complex viscosity, η^* , is shown for the neat, mCNC2, and mCNC3 samples. The measured η^* values before cure (25°C) of neat, mCNC2, and mCNC3 samples are 70.6, 74.3, and 124.0 Pa, respectively. The viscosity is lowest in the neat system, where no fillers are present. Despite fillers in mCNC2, the lack of compatibility between the matrix and the filler yields a material with minimal elastic behavior (compared to mCNC3). Without proper modification to the naturally hydrophilic surface, the particles are likely to aggregate, forming large clusters within the polymer matrix.⁵ In contrast, mCNC3 contained CNCs with a higher functionalization level and showed a higher η^* value at room temperature. The surface modification allows for enhanced dispersion in the non-polar polymer, forming a network of CNCs, rather than isolated aggregates.

A complete evolution of the viscoelastic properties of the neat, mCNC2, and mCNC3 samples are shown in Figure 6. During the ramp to reach 90°C, all samples show an immediate decrease in G' due to increased thermal motion. While all samples show a similar trend in G' , G' is higher (at $T < 90^\circ\text{C}$) for mCNC3 due to an arranged network of the CNCs. In the mCNC2 sample, G' is higher than that of the neat resin due to the presence of fillers. After 13 minutes at 90°C ($t_{\text{age}}=26$ min), G' for mCNC3 drops slightly below that of mCNC2. This decrease in storage modulus is possibly due to a shift from a well-dispersed arrangement of CNCs into a more aggregated state. This shift in properties was also observed during XPCS measurements through the changes shown in v_d (Figure 4).

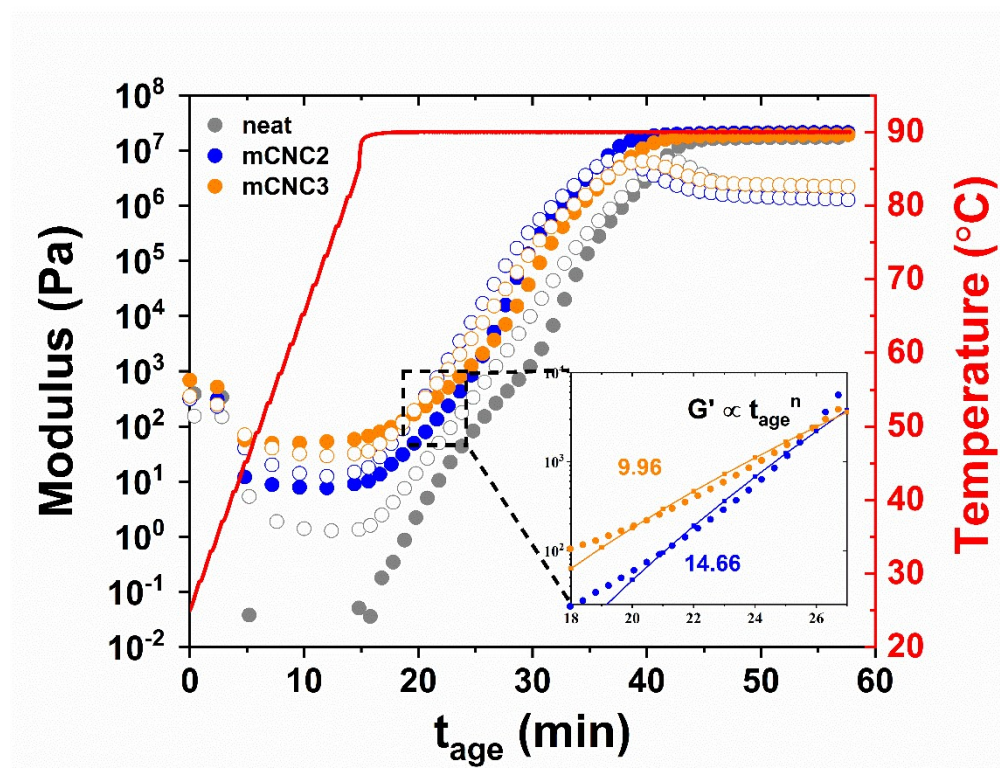


Figure 6. Rheological measurements of the viscoelastic properties of neat EPON 828 and mCNC samples during thermal cure. The storage modulus (G') values are denoted as solid symbols and loss modulus (G'') as open symbols. The inset graph showcases the power-law dependence ($G' \propto t_{\text{age}}^n$) from $t_{\text{age}} = 18\text{--}27$ min.

Further, between the t_{age} range of 35–41 min, a crossover of G' and G'' occur for all samples. The cross over time (t_{gel}) indicates the onset of a viscoelastic network. Gelation occurs when particles percolate and span space to form an interconnected network. Regarding the epoxy crosslinks, gelation is initiated by applying heat and progresses through a chemical crosslinking process. During the reaction, polymer chains link to form a 3D network. The measured t_{gel} values (which include a ramp time of 13 min from 25 to 90°C) of neat, mCNC2, and mCNC3 are 41.1, 35.8, and 37.30 minutes, respectively.

For mCNC3, the well-dispersed system of CNC's has a higher elastic modulus at $t_{\text{age}}=13$ min (90°C). As a result, the dispersed particle system slows down the rate of crosslinking, leading to a gelation time higher than that of mCNC2. For mCNC2, the value of G' at $t_{\text{age}}=13$ min is higher than that of the neat resin but lower than that of mCNC3. However, the aggregated state gives rise to a higher crosslinking rate (than mCNC3), decreasing t_{gel} to a value of 35.8 minutes. Figure 6 (inset) illustrates this point where G' is plotted as a function of time at the beginning of the curing reaction. As shown in the inset, G' is higher for mCNC3, but the rate at which it grows is slower (as seen from the power-law exponent), giving rise to a higher t_{gel} value.

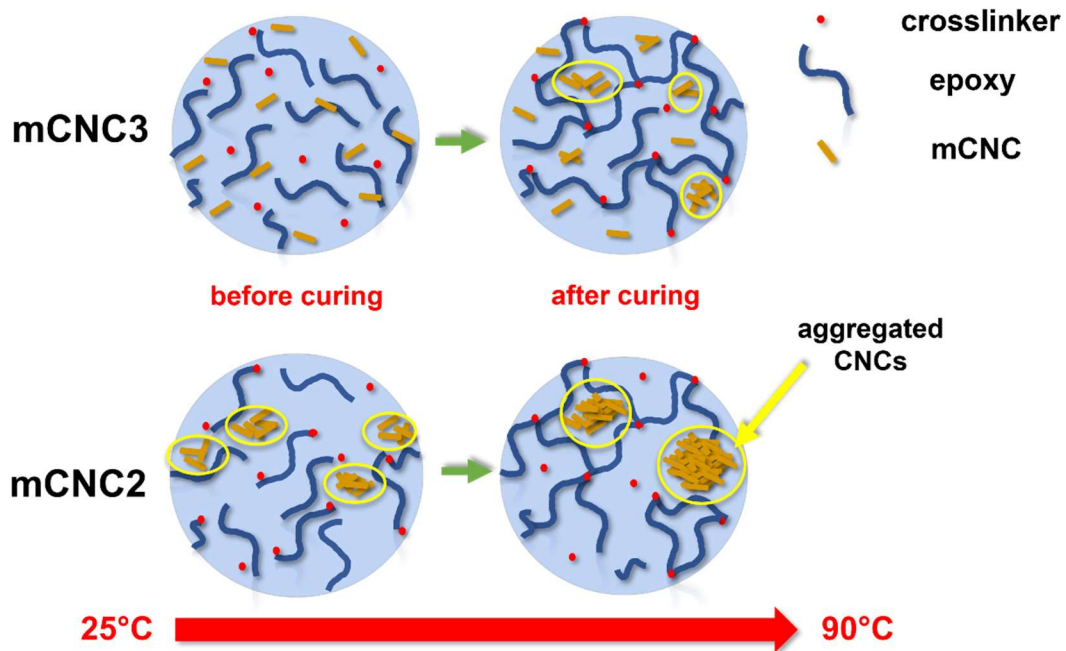


Figure 7. A schematic diagram of the structural changes in mCNC2 and mCNC3 at the beginning and end of the cure.

As the cure progresses, each system reaches the same final G' value despite the initial structure of CNCs present in each sample. A schematic of the possible change in the structure of the mCNCs is shown in Figure 7. A nanoscale analysis (XPCS and SAXS) of the neat resin is not possible due to the lack of scattering from the sample. However, the similar plateau value of v_d shown in Figure

4 and the final G' values in Figure 6 suggest that the final nanoscale properties of the neat, mCNC2, and mCNC3 are similar. Furthermore, the equivalent values of G' also indicate that the crosslinked resin ultimately dominates the macroscopic properties of the composite. Thus, the changes on the nanoscale observed in XPCS correlate well with the macroscopic changes observed in the rheological and DSC studies, showcasing XPCS as a valuable tool in understanding and characterizing CNCs based composite materials.

In summary, three techniques have been used to understand the curing kinetics of a highly filled epoxy-CNC composite. DSC directly measures the kinetics of the crosslinking process through changes in heat flow. Curing rheology measures the elastic properties of the system as the crosslinked network is formed, and XPCS tracks the nanoscale motion of the mCNCs embedded within the network. While each technique measures different 'features' of the system, this study highlights important relationships and trends amongst the three methods and measured values. The degree of cure (α - DOC) is a well-known relationship used to quantify residual cure within crosslinked networks and compares the results obtained from XPCS and DSC. Additionally, a fractional G' ($F_{G'}$) is calculated to showcase the evolution of G' in a similar fashion. The DOC and $F_{G'}$ can be described through the following relationships:

$$\alpha_{DSC} = \frac{H(t)}{H_{total}} \quad (5)$$

$$\alpha_{XPCS} = \frac{v_{d0} - v_d(t)}{v_{d0} - v_{d\infty}} \quad (6)$$

$$F_{G'} = \frac{G'(t) - G'_{t0}}{G'_{\infty} - G'_{t0}} \quad (7)$$

The DOC and $F_{G'}$ are shown in Figure 8 and were calculated at the isothermal cure (90°C). It is well known that many epoxy systems will start polymerization during ramp-up, before curing

temperature ($<90^{\circ}\text{C}$). However, the number of crosslinks formed is negligible at $T < 90^{\circ}\text{C}$. The DOC and $F_{G'}$ comparison obtained from the XPCS, DSC, and rheology under isothermal conditions was presented in this research and established a good correlation among the three methods.

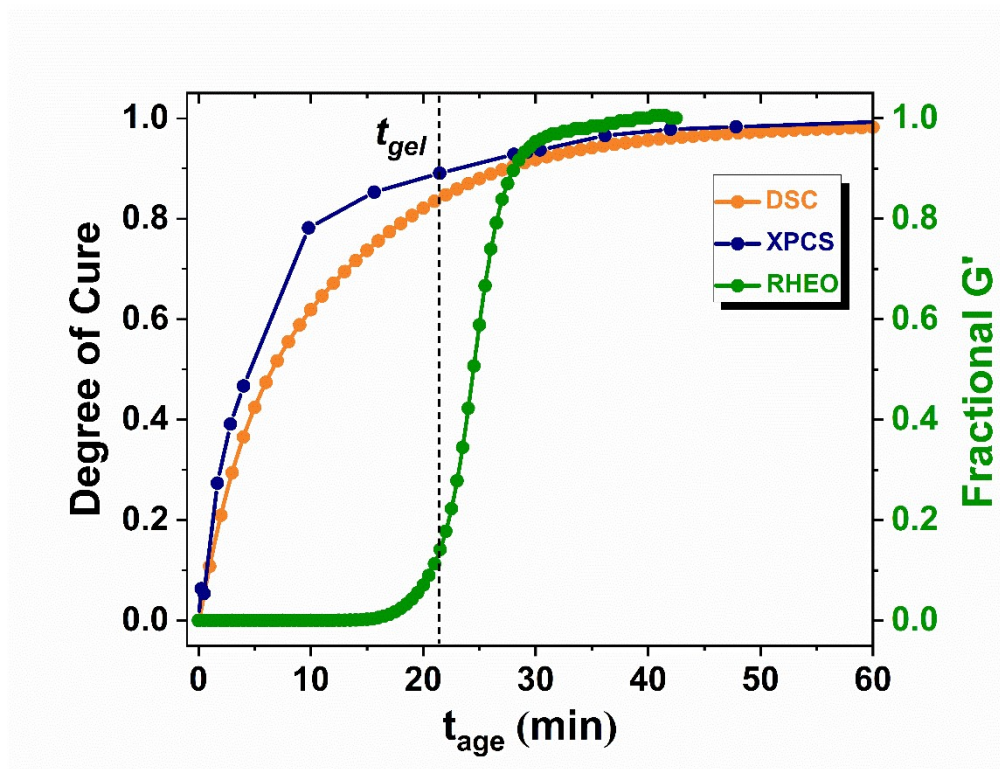


Figure 8. A comparison plot showcasing the overall progression of cure using the three techniques: DSC, XPCS, and rheology for mCNC3.

Figure 8 highlights the gelation time of mCNC3 as it relates to the DOC. For mCNC3, t_{gel} occurs at a DOC of 0.84 (DSC) or 0.88 (XPCS). While XPCS does not technically measure the dynamics of the crosslinked resin, the similar DOC values at gelation indicate that XPCS is a valuable tool in understanding the dynamics of fillers and tracking the crosslinking reaction of thermosetting resins. This correlation supports in situ cure monitoring during the fabricating process using XPCS

and rheology. On the other hand, XPCS provides critical information on the filler dynamics in resin composite.

CONCLUSIONS

XPCS is employed to characterize and understand the evolution of morphology and dynamics during the thermal cure of a highly filled mCNC thermoset composite. Functionalized CNCs (at varying surface modification levels) were incorporated into an epoxy resin with the best dispersion achieved at the higher level of modification (mCNC3). The nanoscale dynamics of mCNC's in the epoxy matrix were characterized through the two-time correlation functions during the thermal cure cycle. mCNC2 and mCNC3 exhibited ballistic, hyper-diffusive motion ($\tau_0 \propto q^{-1}$, $\gamma > 1$) throughout the cure. While both modified systems display similar dynamical properties, the influence of surface modification is reflected quantitatively with differences in power-law exponents, n , where $v_d \propto t_{\text{age}}^{-n}$. The slower dynamics observed in mCNC3 ($n=2.73$) (compared to mCNC2 ($n=4.35$)) suggest the sample contained well-dispersed CNCs, resulting in a network formation of the functionalized particles.

Nanoscale dynamics and macroscopic rheology of the composites are strongly influenced by the curing reaction. Once curing begins, for mCNC3, v_d continues to decrease due to the crosslink's formation in the epoxy resin, but the magnitude of v_d drops below mCNC2. A similar shift can also be observed during the curing rheology studies, where the magnitude of G' shifts to a value lower than G' for mCNC2. Finally, at the end of the cure cycle, both mCNC2 and mCNC3 exhibit identical nanoscale and macroscale properties. Two significant conclusions can be shown from this study. 1) For mCNC3, heat-induced aggregation during the thermal cure results in the formation of a more aggregated cluster, similar to that of mCNC2. 2) While fillers were present at high loadings, the crosslinked resin dominated the final macroscopic properties.

The results from XPCS provide quantitative information regarding the cure behavior of the CNC-epoxy composite and correlate well with macroscopic properties obtained from DSC and curing rheology experiments. XPCS studies provide a nanoscale view of the changes during the thermal cure and demonstrate how the CNC functionalization levels influence the nanoscale structure and crosslinking kinetics. This technique can explain changes on the nanoscale related to the relaxation and spatial organization of CNCs. The control of nanofillers' organization and arrangement can be challenging but is necessary to produce enhanced polymeric nanocomposites and expand the application of the materials.

MATERIALS AND METHODS

All chemicals and solvents were purchased from Sigma-Aldrich at the highest purity available and used without further purification. Spray-dried CNCs in powder form were used as received from the manufacturer (CelluForce, Montreal, Canada). EPON 828 and EPIKURE 3300 (Hexion) (Figure S2) served as the 2-part resin system to prepare the nanocomposites.

Modification of lauroyl fatty acids on CNC

Dried CNC (3wt%) was added into toluene and sonicated for 1 hr. until a uniform dispersion was achieved. The dispersion was then transferred into a three-neck round bottom flask, fitted with a condenser, and placed into a silicone oil bath. Pyridine (base) was added at 2wt% (10g [0.126 mol]), and the toluene-CNC dispersion was heated to 90°C. Lauroyl chloride was added drop by drop at two different levels (7wt% (35 g [0.160 mol]) and 10wt% (50 g [0.229 mol])). The reaction was then refluxed to 110°C (under nitrogen atmosphere) with constant stirring for 1 hr. After 1 hour, the flask was removed from the heat, and ethanol was added to terminate the reaction. The modified CNCs are extracted by thoroughly washing with ethanol and acetone three times. The

modified CNCs were then dried and stored at room temperature for further characterization and processing.

Composite Formation

As shown in Figure 1, the composite formation involves 4 steps: 1) addition of the mCNCs into the resin, 2) sonication of the resin-mCNC mixture, 3) addition of the crosslinking agent, 4) high speed centrifugal mixing of the resin-mCNC-crosslinker mixture. In this study, the neat sample and the composite systems containing three different levels of surface modification on the CNC are prepared. The final CNC concentration (both modified and unmodified) for all studies of the composite was set at 15.5vol% (10wt%), and the samples will be referred to as mCNC1 (neat CNCs), mCNC2 (low-level modification), and mCNC3 (high-level modification).

Characterization Methods

Differential Scanning Calorimetry

The thermal transitions of the CNC-epoxy composite were analyzed using differential scanning calorimetry (DSC). DSC was performed using a DSC-250 (TA Instruments) under a constant N₂ flow of 50mL/min. The uncured sample was placed into a sealed Tzero aluminum hermetic DSC pan, where sample weight varied from 9-12mg. For each sample, the isothermal measurements were performed to determine thermal transitions during cure. The isothermal measurements followed similar conditions to that of the XPCS in-situ curing measurements. Each sample was placed into the DSC at 25°C and heated at 5°C/min 90°C. The sample was held at the isothermal temperature for 120 minutes.

Rheology

Rheological characterization of the CNC-epoxy composite system was carried out using an Anton Paar MCR 302 stress-controlled rheometer. A disposable parallel plate system was used for all experiments (25mm top plate). All experiments were carried out in the linear viscoelastic regime (0.1-1% strain) at a frequency of 1 Hz. The storage modulus (G'), loss modulus (G''), and complex viscosity (η^*) were determined over time at 90°C. The measurements were performed at similar conditions as the XPCS measurements.

X-ray Photon Correlation Spectroscopy & Small-Angle X-ray Scattering

Simultaneous small-angle x-ray scattering (SAXS) and XPCS measurements were used to investigate the changes in structure and dynamics during the thermal cure of the mCNC-epoxy prepreg. The SAXS and XPCS measurements were performed at the Coherent Hard X-ray scattering beamline (CHX, 11ID) at Brookhaven National Laboratory (NSLS-II). The curing agent is added to the pre-mixed mCNC-epoxy mixture, and the samples are immediately loaded into an aluminum holder between two Kapton windows (diameter= 3mm). The sample thickness is 2 mm. The samples were loaded at room temperature (25°C), ramped at 5°C/min to 90°C, and held at that temperature for 1.5 hours. For SAXS and XPCS measurements, a partially coherent X-ray beam with a size of 40 x 40 μm^2 (FWHM) and x-ray energy of 9.646 keV (wavelength, $\lambda_{\text{x-ray}} = 1.284 \text{ \AA}^{-1}$) was used. All data were collected over a q-range of 0.0006-0.025 \AA^{-1} (with the wave vector amplitude $q=4\pi\sin(\theta)/\lambda_{\text{x-ray}}$), corresponding to the scattering angle 2θ . The exposure time for each frame varied from 0.02-2.5s, and 500 frames were collected for each measurement. The combinations of exposure time and X-ray beam attenuation (by double-sided polished silicon wafers) were chosen to keep the X-ray dose below the threshold for beam damage, i.e., in the regime where the dynamics were found to be dose-independent. In addition, the sample position

was shifted laterally across the beam by $\sim 75\mu\text{m}$ after each measurement. All data were analyzed using python code and the computing infrastructure of the CHX beamline (NSLS-II GitHub).

The structural dynamics observed during XPCS measurements can be quantified using the autocorrelation function g_2 ^{65,66}.

$$g_2(q, \tau) = \frac{\langle I(q, t) \cdot I(q, t + \tau) \rangle_q}{\langle I(q, t) \rangle_q^2} \quad (1)$$

In Equation 1, the angular brackets indicate the ensemble averaging over the scattering volume and assume that the dynamics are in equilibrium. The intensity is measured over the wave vector q , at time t , and delay time τ . The angular brackets in Equation 1 indicate both the average over all pixels in the scattering pattern with similar wave vector amplitude ($q \pm \text{A}^{-1}$) and the average over t , thus assuming equilibrium dynamics. This study collected data over a q range of 0.0006-0.025 A^{-1} . This q -range allows us to study dynamics at length scales (nm to μm) relevant to changes occurring within thermosetting composites³³. Experimental data is often described using the Kohlrausch-Williams-Watts (KWW) equation, a stretched exponential function⁶⁷.

$$g_2(q, \tau) = 1 + \beta(q) \exp[-2(\tau/\tau_0(q))^\gamma] \quad (2)$$

Here, β is the setup dependent contrast factor (determined as $\beta \approx 0.12$ using a static sample), $\tau_0(q)$ is the relaxation time, and γ is the stretching exponent. The KWW function is widely used to describe relaxations in systems that do not obey simple exponential dynamics⁶⁸. As stated above, Equation 1 assumes that dynamics are in equilibrium, meaning the dynamics timescales are independent of the measurement time t . If different regions relax on different time scales in the sample, then out-of-equilibrium dynamics must be considered and accounted for in the calculation of g_2 . Many systems display such non-equilibrium dynamics^{33,36,51,69}, and time-resolved

experiments can monitor their behavior. In XPCS, this behavior is measured using the two-time autocorrelation function, where the correlation analysis must be performed explicitly as a function of time. The two-time correlation function measures out-of-equilibrium dynamics using the following relationship⁷⁰:

$$C(q, t_1, t_2) = \frac{\langle I(q, t_1) \cdot I(q, t_2) \rangle_q}{\langle I(q, t_1) \rangle_q \cdot \langle I(q, t_2) \rangle_q} \quad (3)$$

An average time or "age" of the sample can be defined as $t_{\text{age}} = t_1 + t_2 / 2$ and represents the time along the $t_1 = t_2$ diagonal on the two-time autocorrelation plot. Additionally, delay time τ is now described as $|t_2 - t_1|$. If the dynamics is quasi-stationary over an age interval $t_{\text{age}} \pm \Delta t_{\text{age}}$, a one-time correlation function

$$g_2(q, t_{\text{age}}, \tau) = \frac{\langle I(q, t_{\text{age}} - \frac{\tau}{2}) \cdot I(q, t_{\text{age}} + \frac{\tau}{2}) \rangle_{q, t_{\text{age}} \pm \Delta t_{\text{age}}}}{\langle I(q, t_{\text{age}} - \frac{\tau}{2}) \rangle_{q, t_{\text{age}} \pm \Delta t_{\text{age}}} \cdot \langle I(q, t_{\text{age}} + \frac{\tau}{2}) \rangle_{q, t_{\text{age}} \pm \Delta t_{\text{age}}}} \quad (4)$$

can be obtained from the two-time correlation function in Equation (3), which can be fitted with Equation (2) for quantitative analysis. During the thermal cure of the mCNC samples, time and temperature-dependent changes occur. The two-time correlation plots showcase the changes in dynamics and qualitatively provide information about the sample's out-of-equilibrium dynamics within that specific snapshot or measurement window. The average time or age time ($t_{\text{age}} = (t_1 + t_2) / 2$) is measured along the distance of the diagonal (denoted with solid black-see Figure S7a). Along the diagonal, $t_1 = t_2$. The intensities extracted from two speckle patterns (collected at times t_1 and t_2) are used in the calculation of g_2 (equation 3) and the color variations represent the values of g_2 .

AUTHOR INFORMATION

*Email: srama@eng.famu.fsu.edu

Phone: 001 (850) 410-6159

ACKNOWLEDGMENTS

R. Haney would like to acknowledge funding from the NSF FAMU CREST center award # 1735968 for the current work. R. Haney would also like to thank the Materials & Manufacturing Directorate of the Air Force Research Laboratory for characterization equipment. S. Ramakrishnan and R. Kollarigowda would like to acknowledge funding from Department of Defense proposal number 76182-MS-REP, agreement number W911NF-20-1-0263. This research used resources and the Coherent Hard X-ray Scattering (CHX, 11-ID) beamline of the National Synchrotron Light Source II, a U.S. Department of Energy (DOE) Office of Science User Facility operated for the DOE Office of Science by Brookhaven National Laboratory under Contract No. DE- SC0012704.

ASSOCIATED CONTENT

Supporting Information

This information is available free of charge.

Transmission electron micrograph of neat (unmodified) cellulose nanocrystals, Figure S1 (PDF).

Chemical structures of the epoxy resin and curing agent (2-part resin system) Figure S2 (PDF).

Fourier transform infrared spectroscopy and x-ray diffraction patterns for neat and modified cellulose nanocrystal, Figure S3 (PDF).

The X-ray diffraction pattern-based CI values for the neat and modified CNCs (7 and 10%) Table S1 (PDF).

Suspensions of unmodified and modified cellulose nanocrystals (2wt%) in water, ethanol, dimethyl sulfoxide, acetone, toluene, and cyclohexane, Figure S4 (PDF).

2D small angle X-ray scattering patterns for mCNC2 and mCNC3 at 25°C, Figure S5 (PDF).

Intensity (I) vs. q plots for mCNC2 and mCNC3 during the thermal cure at 77°C and 90°C with the corresponding power law fits (p) where $I(q) \propto q^{-p}$, Figure S6 (PDF).

Relaxation time (τ_0) q dependence and corresponding fits, where $\tau_0 \propto q^{-n}$ at various stages of the cure of the mCNC2 sample, Figure S7 (PDF).

XPCS two-time correlation functions ($q=0.0061 \text{ \AA}^{-1}$) during the thermal cure of mCNC2 and mCNC3, Figure S8 (PDF).

The KWW stretching exponent, γ , for mCNC2 and mCNC3 as a function of t_{age} from the fits of the correlation functions ($q=0.0061 \text{ \AA}^{-1}$) shown in Figure 3, Figure S9 (PDF).

The evolution of the complex viscosity during the thermal cure of the neat epoxy resin, mCNC2, and mCNC3 samples, Figure S10 (PDF).

REFERENCES

- (1) Jin, F.-L.; Li, X.; Park, S.-J. Synthesis and Application of Epoxy Resins: A Review. *Journal of Industrial and Engineering Chemistry* **2015**, *29*, 1–11. <https://doi.org/10.1016/j.jiec.2015.03.026>.
- (2) Jiang, W.; Jin, F.-L.; Park, S.-J. Thermo-Mechanical Behaviors of Epoxy Resins Reinforced with Nano-Al₂O₃ Particles. *Journal of Industrial and Engineering Chemistry* **2012**, *18* (2), 594–596. <https://doi.org/10.1016/j.jiec.2011.11.140>.
- (3) Huang, H.; Sheng, X.; Tian, Y.; Zhang, L.; Chen, Y.; Zhang, X. Two-Dimensional Nanomaterials for Anticorrosive Polymeric Coatings: A Review. *Ind. Eng. Chem. Res.* **2020**, *59* (35), 15424–15446. <https://doi.org/10.1021/acs.iecr.0c02876>.
- (4) Sasidharan, S.; Anand, A. Epoxy-Based Hybrid Structural Composites with Nanofillers: A Review. *Ind. Eng. Chem. Res.* **2020**, *59* (28), 12617–12631. <https://doi.org/10.1021/acs.iecr.0c01711>.

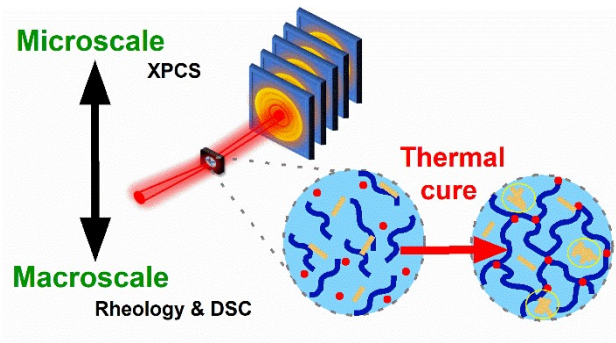
- (5) Pruksawan, S.; Samitsu, S. Toughening Effect of Rodlike Cellulose Nanocrystals in Epoxy Adhesive. *ACS Applied Polymer Materials* **2020**, *2* (3), 1234–1243. <https://doi.org/10.1021/acsapm.9b01102>.
- (6) Pandey, J. K.; Nakagaito, A. N.; Takagi, H. Fabrication and Applications of Cellulose Nanoparticle-Based Polymer Composites. *Polymer Engineering & Science* **2013**, *53* (1), 1–8. <https://doi.org/10.1002/pen.23242>.
- (7) Trache, D.; Tarchoun, A. F.; Derradji, M.; Hamidon, T. S.; Masruchin, N.; Brosse, N.; Hussin, M. H. Nanocellulose: From Fundamentals to Advanced Applications. *Front. Chem.* **2020**, *8*. <https://doi.org/10.3389/fchem.2020.00392>.
- (8) Zhang, Z.; Lu, S.; Cai, R.; Tan, W. Rapid Water-Responsive Shape Memory Films for Smart Resistive Bending Sensors. *Nano Today* **2021**, *38*, 101202. <https://doi.org/10.1016/j.nantod.2021.101202>.
- (9) Zhang, Z.; Yang, D.; Yang, H. A Hydrophobic Sisal Cellulose Microcrystal Film for Fire Alarm Sensors. *Nano Letters* **2021**, *21* (5), 2104–2110. <https://doi.org/10.1021/acs.nanolett.0c04789>.
- (10) Foster, E. J.; Moon, R. J.; Agarwal, U. P.; Bortner, M. J.; Bras, J.; Camarero-Espinosa, S.; Chan, K. J.; Clift, M. J. D.; Cranston, E. D.; Eichhorn, S. J.; Fox, D. M.; Hamad, W. Y.; Heux, L.; Jean, B.; Korey, M.; Nieh, W.; Ong, K. J.; Reid, M. S.; Renneckar, S.; Roberts, R.; Shatkin, J. A.; Simonsen, J.; Stinson-Bagby, K.; Wanasekara, N.; Youngblood, J. Current Characterization Methods for Cellulose Nanomaterials. *Chem. Soc. Rev.* **2018**, *47* (8), 2609–2679. <https://doi.org/10.1039/C6CS00895J>.
- (11) Tavakolian, M.; Jafari, S. M.; van de Ven, T. G. M. A Review on Surface-Functionalized Cellulosic Nanostructures as Biocompatible Antibacterial Materials. *Nano-Micro Lett.* **2020**, *12* (1), 73. <https://doi.org/10.1007/s40820-020-0408-4>.
- (12) Khanjanzadeh, H.; Behrooz, R.; Bahramifar, N.; Gindl-Altmutter, W.; Bacher, M.; Edler, M.; Griesser, T. Surface Chemical Functionalization of Cellulose Nanocrystals by 3-Aminopropyltriethoxysilane. *International Journal of Biological Macromolecules* **2018**, *106*, 1288–1296. <https://doi.org/10.1016/j.ijbiomac.2017.08.136>.
- (13) Wan, W. Direct Surface Functionalization of Cellulose Nanocrystals with Hyperbranched Polymers through the Anionic Polymerization for PH-Responsive Intracellular Drug Delivery. *ACS Sustainable Chemistry & Engineering* **2019**, *7* (23), 19202–19212.
- (14) Fatona, A.; Berry, R. M.; Brook, M. A.; Moran-Mirabal, J. M. Versatile Surface Modification of Cellulose Fibers and Cellulose Nanocrystals through Modular Triazinyl Chemistry. *Chem. Mater.* **2018**, *30* (7), 2424–2435. <https://doi.org/10.1021/acs.chemmater.8b00511>.
- (15) Wang, Y.; Wang, X.; Xie, Y.; Zhang, K. Functional Nanomaterials through Esterification of Cellulose: A Review of Chemistry and Application. *Cellulose* **2018**, *25* (7), 3703–3731. <https://doi.org/10.1007/s10570-018-1830-3>.
- (16) Trinh, B. M.; Mekonnen, T. Hydrophobic Esterification of Cellulose Nanocrystals for Epoxy Reinforcement. *Polymer* **2018**, *155*, 64–74. <https://doi.org/10.1016/j.polymer.2018.08.076>.
- (17) Introduction and Objectives. In *Esterification of Polysaccharides*; Heinze, T., Liebert, T., Koschella, A., Eds.; Springer Laboratory; Springer: Berlin, Heidelberg, 2006; pp 1–3. https://doi.org/10.1007/3-540-32112-8_1.

- (18) Freire, C.; Silvestre, A.; Neto, C.; Rocha, R. M. A. An Efficient Method for Determination of the Degree of Substitution of Cellulose Esters of Long Chain Aliphatic Acids. *Cellulose* **2005**, *12*, 449–458. <https://doi.org/10.1007/s10570-005-2203-2>.
- (19) Abraham, E.; Kam, D.; Nevo, Y.; Slattegard, R.; Rivkin, A.; Lapidot, S.; Shoseyov, O. Highly Modified Cellulose Nanocrystals and Formation of Epoxy-Nanocrystalline Cellulose (CNC) Nanocomposites. *ACS Appl. Mater. Interfaces* **2016**, *8* (41), 28086–28095. <https://doi.org/10.1021/acsami.6b09852>.
- (20) Grossiord, N.; Loos, J.; Regev, O.; Koning, C. E. Toolbox for Dispersing Carbon Nanotubes into Polymers To Get Conductive Nanocomposites. *Chem. Mater.* **2006**, *18* (5), 1089–1099. <https://doi.org/10.1021/cm051881h>.
- (21) Alhabill, F. N.; Ayoob, R.; Andritsch, T.; Vaughan, A. S. Influence of Filler/Matrix Interactions on Resin/Hardener Stoichiometry, Molecular Dynamics, and Particle Dispersion of Silicon Nitride/Epoxy Nanocomposites. *J Mater Sci* **2018**, *53* (6), 4144–4158. <https://doi.org/10.1007/s10853-017-1831-x>.
- (22) Singh, M.; Pandey, J. Effect of Particle Surface Treatment on Dielectric Properties of Epoxy-Alumina Nano-Composites; 2016.
- (23) Kothmann, M.; Rios de Anda, A.; Koepfel, A.; Zeiler, R.; Tauer, G.; Zhang, Z.; Altstädt, V. The Effect of Dispersion and Particle–Matrix Interactions on the Fatigue Behavior of Novel Epoxy/Halloysite Nanocomposites; 2019; pp 121–155. <https://doi.org/10.3139/9781569906361.004>.
- (24) Chang, T. D.; Carr, S. H.; Brittain, J. O. Studies of Epoxy Resin Systems: Part B: Effect of Crosslinking on the Physical Properties of an Epoxy Resin. *Polymer Engineering & Science* **1982**, *22* (18), 1213–1220. <https://doi.org/10.1002/pen.760221807>.
- (25) Kumar, A.; Sundararaghavan, V.; Browning, A. Study of Temperature Dependence of Thermal Conductivity in Cross-Linked Epoxies Using Molecular Dynamics Simulations with Long Range Interactions. *Modelling and Simulation in Materials Science and Engineering* **2014**, *22*. <https://doi.org/10.1088/0965-0393/22/2/025013>.
- (26) Macan, J.; Brnardić, I.; Ivanković or Opalički, M.; Mencer, H. DSC Study of Cure Kinetics of DGEBA-Based Epoxy Resin with Poly(Oxypropylene) Diamine. *Journal of Thermal Analysis and Calorimetry* **2005**, *81*, 369–373. <https://doi.org/10.1007/s10973-005-0794-3>.
- (27) Hardis, R.; Jessop, J. L. P.; Peters, F. E.; Kessler, M. R. Cure Kinetics Characterization and Monitoring of an Epoxy Resin Using DSC, Raman Spectroscopy, and DEA. *Composites Part A: Applied Science and Manufacturing* **2013**, *49*, 100–108. <https://doi.org/10.1016/j.compositesa.2013.01.021>.
- (28) Roşu, D.; Caşcaval, C. N.; Mustăţă, F.; Ciobanu, C. Cure Kinetics of Epoxy Resins Studied by Non-Isothermal DSC Data. *Thermochimica Acta* **2002**, *383* (1), 119–127. [https://doi.org/10.1016/S0040-6031\(01\)00672-4](https://doi.org/10.1016/S0040-6031(01)00672-4).
- (29) Hickey, C. M. D.; Bickerton, S. Cure Kinetics and Rheology Characterisation and Modelling of Ambient Temperature Curing Epoxy Resins for Resin Infusion/VARTM and Wet Layup Applications. *J Mater Sci* **2013**, *48* (2), 690–701. <https://doi.org/10.1007/s10853-012-6781-8>.
- (30) Parameswaranpillai, J.; George, A.; Pionteck, J.; Thomas, S. Investigation of Cure Reaction, Rheology, Volume Shrinkage and Thermomechanical Properties of Nano-TiO₂ Filled Epoxy/DDS Composites. *Journal of Polymers* **2013**, *2013*, e183463. <https://doi.org/10.1155/2013/183463>.

- (31) Artmann, A.; Bianchi, O.; Soares, M. R.; Nunes, R. C. R. Rheokinetic Investigations on the Thermal Cure of Phenol-Formaldehyde Novolac Resins. *Materials Science and Engineering: C* **2010**, *30* (8), 1245–1251. <https://doi.org/10.1016/j.msec.2010.07.008>.
- (32) Wu, F.; Zhou, X.; Yu, X. Reaction Mechanism, Cure Behavior and Properties of a Multifunctional Epoxy Resin, TGDDM, with Latent Curing Agent Dicyandiamide. *RSC Adv.* **2018**, *8* (15), 8248–8258. <https://doi.org/10.1039/C7RA13233F>.
- (33) Yavitt, B. M.; Salatto, D.; Huang, Z.; Koga, Y. T.; Endoh, M. K.; Wiegart, L.; Poeller, S.; Petrash, S.; Koga, T. Revealing Nanoscale Dynamics during an Epoxy Curing Reaction with X-Ray Photon Correlation Spectroscopy. *Journal of Applied Physics* **2020**, *127* (11), 114701. <https://doi.org/10.1063/1.5141488>.
- (34) Srivastava, S.; Kandar, A. K.; Basu, J. K.; Mukhopadhyay, M. K.; Lurio, L. B.; Narayanan, S.; Sinha, S. K. Complex Dynamics in Polymer Nanocomposites. *Phys. Rev. E* **2009**, *79* (2), 021408. <https://doi.org/10.1103/PhysRevE.79.021408>.
- (35) Grein-Iankovski, A.; Riegel-Vidotti, I. C.; Simas-Tosin, F. F.; Narayanan, S.; Leheny, R. L.; Sandy, A. R. Exploring the Relationship between Nanoscale Dynamics and Macroscopic Rheology in Natural Polymer Gums. *Soft Matter* **2016**, *12* (46), 9321–9329. <https://doi.org/10.1039/C6SM01492E>.
- (36) Johnson, K.; Wiegart, L.; Abbott, A.; Johnson, E.; Baur, J.; Koerner, H. In Operando Monitoring of Dynamic Recovery in 3D-Printed Thermoset Nanocomposites by XPCS. *Langmuir* **2019**, *35* (26), 8758–8768. <https://doi.org/10.1021/acs.langmuir.9b00766>.
- (37) Nogales, A.; Fluerasu, A. X Ray Photon Correlation Spectroscopy for the Study of Polymer Dynamics. *European Polymer Journal* **2016**, *81*, 494–504. <https://doi.org/10.1016/j.eurpolymj.2016.03.032>.
- (38) Lu, P.; Hsieh, Y.-L. Preparation and Properties of Cellulose Nanocrystals: Rods, Spheres, and Network. *Carbohydrate Polymers* **2010**, *82* (2), 329–336. <https://doi.org/10.1016/j.carbpol.2010.04.073>.
- (39) Sanchez-Botero, L.; Dimov, A.; Li, R.; Smilgies, D.-M.; Hinestroza, J. In Situ and Real-Time Studies, via Synchrotron X-Ray Scattering, of the Orientational Order of Cellulose Nanocrystals during Solution Shearing. *Langmuir* **2018**, *34*. <https://doi.org/10.1021/acs.langmuir.7b04403>.
- (40) Park, S.; Baker, J. O.; Himmel, M. E.; Parilla, P. A.; Johnson, D. K. Cellulose Crystallinity Index: Measurement Techniques and Their Impact on Interpreting Cellulase Performance. *Biotechnol Biofuels* **2010**, *3* (1), 10. <https://doi.org/10.1186/1754-6834-3-10>.
- (41) Reid, M. S.; Villalobos, M.; Cranston, E. D. Benchmarking Cellulose Nanocrystals: From the Laboratory to Industrial Production. *Langmuir* **2017**, *33* (7), 1583–1598. <https://doi.org/10.1021/acs.langmuir.6b03765>.
- (42) Junior de Menezes, A.; Siqueira, G.; Curvelo, A. A. S.; Dufresne, A. Extrusion and Characterization of Functionalized Cellulose Whiskers Reinforced Polyethylene Nanocomposites. *Polymer* **2009**, *50* (19), 4552–4563. <https://doi.org/10.1016/j.polymer.2009.07.038>.
- (43) Highly Modified Cellulose Nanocrystals and Formation of Epoxy-Nanocrystalline Cellulose (CNC) Nanocomposites | ACS Applied Materials & Interfaces <https://pubs.acs.org/doi/abs/10.1021/acsami.6b09852> (accessed 2021 -04 -11).
- (44) Feigin, L.; Svergun, D. *Structure Analysis by Small-Angle X-Ray and Neutron Scattering*, 1st ed.; Springer, 1987.

- (45) Shah, S.; Subramanian, R.; Schweizer, K.; Zukoski, C. Microstructure of Dense Colloid–Polymer Suspensions and Gels. *Journal of Physics: Condensed Matter* **2003**, *15* (27). <https://doi.org/10.1088/0953-8984/15/27/308>.
- (46) Shah, S.; Subramanian, R.; Chen, Y.; Schweizer, K.; Zukoski, C. Scattering Studies of the Structure of Colloid–Polymer Suspensions and Gels. *Langmuir* **2003**, *19* (12), 5128–5136. <https://doi.org/10.1021/la020982g>.
- (47) Mao, Y. Characterization of Nanocellulose Using Small-Angle Neutron, X-Ray, and Dynamic Light Scattering Techniques. *The Journal of Physical Chemistry B* **2017**, *121* (6), 1340–1351. <https://doi.org/10.1021/acs.jpcc.6b11425>.
- (48) Lazzari, S.; Nicoud, L.; Jaquet, B.; Lattuada, M.; Morbidelli, M. Fractal-like Structures in Colloid Science. *Advances in Colloid and Interface Science* **2016**, *235*, 1–13. <https://doi.org/10.1016/j.cis.2016.05.002>.
- (49) Lazzari, S.; Maggioni, G. M.; Soos, M.; Wu, H.; Morbidelli, M. Shear-Stability and Gelation of Inverse Latexes. *Soft Matter* **2013**, *9* (45), 10866–10876. <https://doi.org/10.1039/C3SM51290H>.
- (50) Lehmkuhler, F. Emergence of Anomalous Dynamics in Soft Matter Probed at the European XFEL; 2020. <https://doi.org/10.1073/pnas.2003337117>.
- (51) Torres Arango, M.; Zhang, Y.; Zhao, C.; Li, R.; Doerk, G.; Nykypanchuk, D.; Chen-Wiegart, Y. K.; Fluerasu, A.; Wiegart, L. Ink-Substrate Interactions during 3D Printing Revealed by Time-Resolved Coherent X-Ray Scattering. *Materials Today Physics* **2020**, *14*, 100220. <https://doi.org/10.1016/j.mtphys.2020.100220>.
- (52) Czakkel, O.; Madsen, A. Evolution of Dynamics and Structure during Formation of a Cross-Linked Polymer Gel. *EPL* **2011**, *95* (2), 28001. <https://doi.org/10.1209/0295-5075/95/28001>.
- (53) Bandyopadhyay, R.; Liang, D.; Yardimci, H.; Sessoms, D. A.; Borthwick, M. A.; Mochrie, S. G. J.; Harden, J. L.; Leheny, R. L. Evolution of Particle-Scale Dynamics in an Aging Clay Suspension. *Phys. Rev. Lett.* **2004**, *93* (22), 228302. <https://doi.org/10.1103/PhysRevLett.93.228302>.
- (54) Cipelletti, L.; Manley, S.; Ball, R. C.; Weitz, D. A. Universal Aging Features in the Restructuring of Fractal Colloidal Gels. *Phys. Rev. Lett.* **2000**, *84* (10), 2275–2278. <https://doi.org/10.1103/PhysRevLett.84.2275>.
- (55) Ranka, M.; Varkey, N.; Ramakrishnan, S.; Zukoski, C. Impact of Small Changes in Particle Surface Chemistry for Unentangled Polymer Nanocomposites. *Soft Matter* **2014**, *11*. <https://doi.org/10.1039/C4SM01598C>.
- (56) Guo, H.; Wilking, J. N.; Liang, D.; Mason, T. G.; Harden, J. L.; Leheny, R. L. Slow, Nondiffusive Dynamics in Concentrated Nanoemulsions. *Phys. Rev. E* **2007**, *75* (4), 041401. <https://doi.org/10.1103/PhysRevE.75.041401>.
- (57) Guo, H.; Ramakrishnan, S.; Harden, J. Gel Formation and Aging in Weakly Attractive Nanocolloid Suspensions at Intermediate Concentrations. *The Journal of Chemical Physics* **2011**, *135* (15). <https://doi.org/10.1063/1.3653380>.
- (58) Herzig, E. M.; Robert, A.; van 't Zand, D. D.; Cipelletti, L.; Pusey, P. N.; Clegg, P. S. Dynamics of a Colloid-Stabilized Cream. *Phys. Rev. E* **2009**, *79* (1), 011405. <https://doi.org/10.1103/PhysRevE.79.011405>.
- (59) Cipelletti, L.; Ramos, L.; Manley, S.; Pitard, E.; Weitz, D. A.; Pashkovski, E. E.; Johansson, M. Universal Non-Diffusive Slow Dynamics in Aging Soft Matter. *Faraday Discuss.* **2003**, *123* (0), 237–251. <https://doi.org/10.1039/B204495A>.

- (60) Bouchaud, J.-P.; Pitard, E. Anomalous Dynamical Light Scattering in Soft Glassy Gels. *Eur. Phys. J. E* **2001**, *6* (3), 231–236. <https://doi.org/10.1007/s101890170005>.
- (61) Westwood, A. R. Analysis of the Curing Reactions of Thermosetting Polymers by DSC. In *Thermal Analysis: Volume 3: Organic and Macromolecular Chemistry, Ceramics, Earth Science*; Wiedemann, H. G., Ed.; Birkhäuser: Basel, 1972; pp 169–177. https://doi.org/10.1007/978-3-0348-5775-8_14.
- (62) Cai, H.; Li, P.; Sui, G.; Yu, Y.; Li, G.; Yang, X.; Ryu, S. Curing Kinetics Study of Epoxy Resin/Flexible Amine Toughness Systems by Dynamic and Isothermal DSC. *Thermochimica Acta* **2008**, *473* (1), 101–105. <https://doi.org/10.1016/j.tca.2008.04.012>.
- (63) Malkin, A. Y.; Kulichikhin, S. G.; Kerber, M. L.; Gorbunova, I. Y.; Murashova, E. A. Rheokinetics of Curing of Epoxy Resins near the Glass Transition. *Polymer Engineering & Science* **1997**, *37* (8), 1322–1330. <https://doi.org/10.1002/pen.11778>.
- (64) Mphahlele, K.; Ray, S. S.; Kolesnikov, A. Cure Kinetics, Morphology Development, and Rheology of a High-Performance Carbon-Fiber-Reinforced Epoxy Composite. *Composites Part B: Engineering* **2019**, *176*, 107300. <https://doi.org/10.1016/j.compositesb.2019.107300>.
- (65) Sutton, M.; Mochrie, S. G. J.; Greytak, T.; Nagler, S. E.; Berman, L. E.; Held, G. A.; Stephenson, G. B. Observation of Speckle by Diffraction with Coherent X-Rays. *Nature* **1991**, *352* (6336), 608–610. <https://doi.org/10.1038/352608a0>.
- (66) *Soft-Matter Characterization*; Borsali, R., Pecora, R., Eds.; Springer Netherlands, 2008.
- (67) Madsen, A.; Leheny, R. L.; Guo, H.; Sprung, M.; Czakkel, O. Beyond Simple Exponential Correlation Functions and Equilibrium Dynamics in X-Ray Photon Correlation Spectroscopy. *New J. Phys.* **2010**, *12* (5), 055001. <https://doi.org/10.1088/1367-2630/12/5/055001>.
- (68) Lukichev, A. Physical Meaning of the Stretched Exponential Kohlrausch Function. *Physics Letters A* **2019**, *383* (24), 2983–2987. <https://doi.org/10.1016/j.physleta.2019.06.029>.
- (69) Yavitt, B. Structural Dynamics in UV Curable Resins Resolved by In Situ 3D Printing X-Ray Photon Correlation Spectroscopy. *ACS Applied Polymer Materials* **2020**, *2* (9), 4096–4108. <https://doi.org/10.1021/acsapm.0c00716>.
- (70) Bikondoa, O. On the Use of Two-Time Correlation Functions for X-Ray Photon Correlation Spectroscopy Data Analysis. *Journal of Applied Crystallography* **2017**, *50* (2), 357–368. <https://doi.org/10.1107/S1600576717000577>.



For Table of Contents Only